PERGAMON

Scripta mater. 42 (2000) 761–767

Scripta MATERIALIA

www.elsevier.com/locate/scriptamat

FATIGUE-CRACK GROWTH AND FRACTURE PROPERTIES OF COARSE AND FINE-GRAINED Ti_3SiC_2

C.J. Gilbert[1], D.R. Bloyer[1], M.W. Barsoum,[2], T. El-Raghy[2], A.P. Tomsia[1] and R.O. Ritchie[1]

[1]Materials Sciences Division, Lawrence Berkeley National Laboratory, and Department of Materials Science and Mineral Engineering, University of California, Berkeley, CA

[2]Department of Materials Engineering, Drexel University, Philadelphia, PA

(Received August 16, 1999)
(Accepted in revised form December 4, 1999)

Keywords: Ceramics; Ti_3SiC_2; Mechanical properties; Fracture; Fatigue

Introduction

Barsoum and El-Raghy [1] have recently developed reactive hot-pressing techniques to form bulk, polycrystalline Ti_3SiC_2 from powders of Ti, SiC, and graphite. This ternary carbide, first synthesized by Jeitschko and Nowotny [2] in the late 1960s, exhibits a rather surprising combination of properties. Not only is the ratio of hardness (~4 GPa) to elastic modulus (~320 GPa) more typical of ductile metals [3,4], but recent experimental studies have revealed a range of inelastic deformation modes not typically observed in ceramics [5–9]. These include grain bending, grain buckling, and significant amounts of basal slip at ambient temperatures [9,10]. It has also been shown that Ti_3SiC_2 [5,6,10], and related ternaries [11,12], are exceptionally damage tolerant materials. A dislocation-based model has recently been proposed to explain this exceptional damage tolerance [9]. The basic elements of the model are shear deformation by dislocation arrays, cavitation, creation of dislocation walls and kink boundaries, buckling and delamination. The delaminations and associated damage appear to be contained by the kink boundaries. It is this containment of damage that is believed to play a major role in endowing Ti_3SiC_2 (and by extension related ternary carbides and nitrides) with their damage tolerant properties.

Studies have also revealed the presence of grain bridging and sliding [5,6], but to a much larger degree than observed in well-studied systems such as Al_2O_3, Si_3N_4, and SiC [e.g., 14–16]. Indeed, the deformation processes observed in individual grains of Ti_3SiC_2 seem to enhance grain bridging by increasing pullout distances and suppressing grain rupture. This plasticity, however, also suggests that Ti_3SiC_2 may be susceptible to cyclic-fatigue failures [6]. Damage associated with cyclic loading in many ceramics is generally attributed to cycle-dependent frictional wear at grain bridging sites. As such, ceramic microstructures designed for damage tolerance are generally more prone to cyclic fatigue degradation; this has been well documented in a range of monolithic and composite ceramics [e.g., 16–19]. To date, however, neither the fatigue-crack propagation nor the resistance-curve (R-curve) properties of monolithic Ti_3SiC_2 have been characterized. Therefore, the aim of this work is to investigate damage processes associated with grain bridging under both cyclic and static loading. We specifically compare coarse and fine-grained microstructures, with the ultimate aim of developing an understanding of mechanisms controlling fracture and cyclic fatigue properties in this unusual class of monolithic ceramics.

PII: S1359-6462(99)00427-3

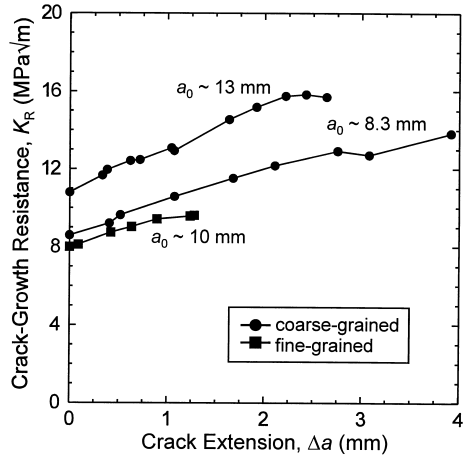

Figure 1. Crack-growth resistance, K_R, is plotted as a function of crack extension, Δa, for both the fine and coarse-grained Ti_3SiC_2 microstructures. The initial flaw size, a_0, is indicated for each measured R-curve.

Experimental Procedures

Ti_3SiC_2 samples were fabricated via a reactive hot isostatic pressing technique starting with TiH_2 (-325 mesh, 99.99%, TIMET, AZ), SiC (grain size, d_m = 20 μm, 99.5%, Atlantic Engineering Equipment, Bergenfield, NJ) and graphite (d_m = 1 μm, 99%, Aldrich Chemicals, Milwaukee, WI). Powders with the desired stoichiometry were mixed in a ball mill, cold-isostatically pressed at 200 MPa, and annealed at 900°C (4 hr) *in vacuo* (10^{-3} Pa) to remove hydrogen. Samples were then sealed in glass under vacuum and hot-isostatically pressed (HIPed) for 4 hr at 1400° and at 1600°C to form the fine- and coarse-grained microstructures, respectively. The coarse-grained structure consisted of large plate-like grains of diameter 50–200 μm and thickness 5–20 μm, whereas grains in the fine-grained microstructure had a diameter of ~7 μm and were ~3 μm thick. X-ray diffraction and scanning electron microscopy (SEM) showed that both structures contained ~2 vol.% unreacted SiC.

Fatigue-crack growth rate behavior was studied in room air (22°C, ~ 45% relative humidity) using polished (~1 μm diamond paste) 2.9 mm thick, 19 mm wide compact-tension C(T) specimens, tested on computer-controlled, servo-hydraulic mechanical testing machines, in general accordance with ASTM standard E647. Specimens were cycled under stress intensity K control, at a frequency of ν = 25 Hz (sine wave) and a load ratio, R ($=K_{min}/K_{max}$) of 0.1, initially with a decreasing stress-intensity range (at a normalized K-gradient ranging of -0.06 to -0.08 mm^{-1}) until measured growth rates were below 10^{-10} m/cycle. The value of the stress-intensity range at this point was used as an operational definition of the fatigue threshold (ΔK_{TH}) below which large cracks are considered dormant. Specimens were subsequently cycled under increasing ΔK conditions with the same K-gradient range up to growth rates approaching 10^{-6} m/cycle.

Cracks were initiated from half-chevron notches to facilitate pre-cracking, which was continued some 1 mm beyond the notch tip prior to data collection. Crack lengths were continuously monitored using unloading elastic-compliance measurements with a 350 Ω strain gauge attached to the back-face of the specimen; readings were checked periodically using a traveling microscope. Optical and compliance measurements were always found to be within ~5%. Data are presented in terms of the growth rate per cycle, da/dN, as a function of the applied stress-intensity range, ΔK ($=K_{max}$ - K_{min}), the latter being computed using standard linear-elastic handbook solutions.

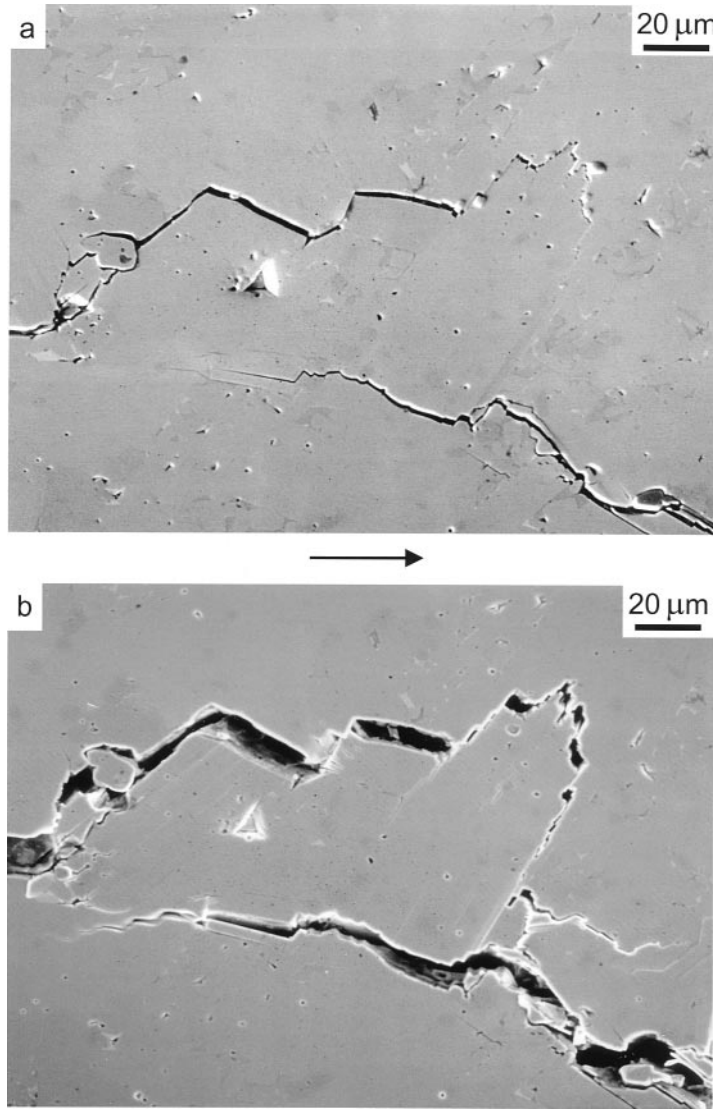

Figure 2. Scanning electron microscope image of crack-wake bridging in the coarse-grained Ti_3SiC_2 microstructure. The same region is depicted in (a) at ~1.7 mm behind the crack tip and in (b) after the crack advanced under monotonic loading such that it is now ~5.4 mm behind the crack tip. Such bridging processes are similar to those observed in well-studied systems like Al_2O_3, Si_3N_4, and SiC. The arrow indicates the direction of crack propagation.

Following fatigue-crack growth characterization, R-curves were measured from the remaining uncracked portion of the specimens. The initial crack length prior to R-curve testing was varied over a wide range; this was primarily to observe any possible large-scale bridging effects. Tests were conducted under displacement control by monotonically loading the C(T) specimens and monitoring subcritical crack growth by both direct optical observation, using a short focal length telescope and back-face strain compliance techniques, the latter using periodic unloads of $<10\%$.

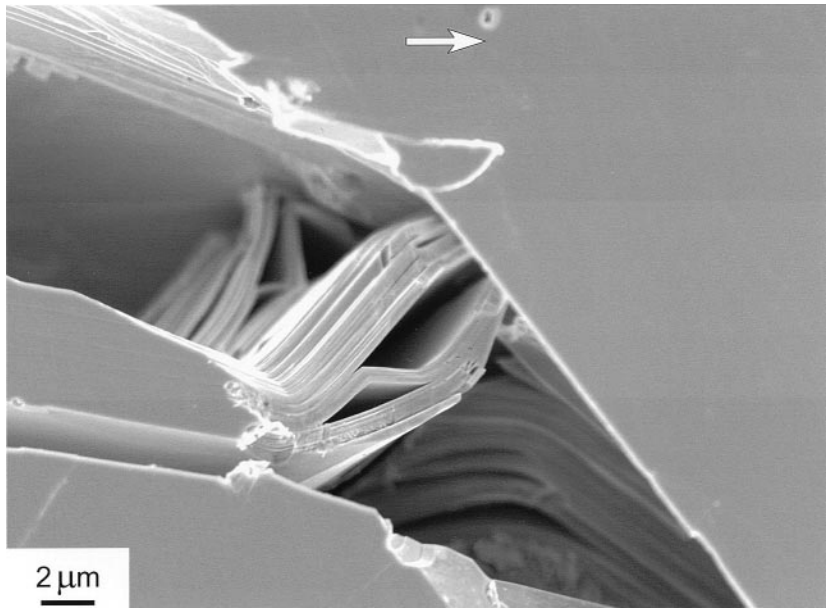

Figure 3. Field-emission scanning electron microscope image of a bridged crack in the coarse-grained Ti_3SiC_2 microstructure. Heavily deformed lamella bridge the crack, and significant amounts of delamination and bending are observed. Such processes are highly unusual in ceramic systems and may, at least partially, account for the extremely high plateau fracture toughnesses (Fig. 1). The arrow indicates the direction of crack propagation.

Crack profiles and fracture surfaces of selected fatigue and R-curve samples were analyzed both optically and in a field-emission scanning electron microscope (FESEM), with the objective of elucidating the salient mechanisms of failure.

Results and Discussion

R-Curve Measurements

Both the fine and coarse-grained microstructures exhibited substantial rising R-curve behavior (Fig. 1). The R-curve for the fine-grained (3–10 μm) Ti_3SiC_2 initiated at ~8 MPa$\sqrt{}$m, and rose to ~9.5 MPa$\sqrt{}$m after ~1.5 mm of crack extension. In this test, the initial flaw was a fatigue crack (~10 mm long), which had been grown at progressively decreasing rates to $\sim 10^{-10}$ m/cycle; despite this, it is conceivable that the high initiation toughness value was associated with some degree of residual bridging in the pre-crack.

The corresponding coarse-grained Ti_3SiC_2 exhibited even higher toughness (Fig. 1). Cracking initiated at ~8.5 MPa$\sqrt{}$m in the first sample, with the crack-growth resistance rising to ~14 MPa$\sqrt{}$m after ~4 mm of crack extension; cracking initiated at ~11 MPa$\sqrt{}$m in the second sample and grew up to ~16 MPa$\sqrt{}$m after ~2.7 mm of crack extension. It should be noted that the initial flaw size appeared to affect the initiation toughness, which again may be associated with residual bridging in the pre-crack.

Consistent with its higher toughness, crack paths in the coarse-grained Ti_3SiC_2 were significantly more tortuous than those in the fine-grained material. SEM examination of the crack-microstructure interactions in the coarse-grained Ti_3SiC_2 revealed significant crack-wake bridging (Fig. 2). The same region is depicted in Fig. 2a at ~1.7 mm behind the crack tip and, after the crack advanced under

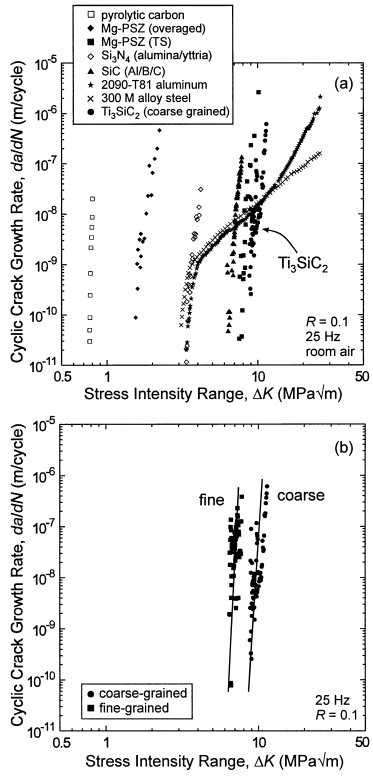

Figure 4. Cyclic-fatigue crack growth rates, *da/dN*, are plotted as a function of the applied stress-intensity range, ΔK. In (a), fatigue properties of the coarse-grained Ti_3SiC_2 is compared to behavior in a range of metals and ceramics. Compared to other ceramics, cyclic-crack growth rates in the Ti_3SiC_2 are low and the fatigue threshold is very high. In (b), fatigue properties of the coarse and fine-grained Ti_3SiC_2 are compared. Typical of ceramics, fatigue-crack growth rates scale directly with fracture toughness.

monotonic loading, in Fig. 2b at ~5.4 mm behind the tip. Evidence for both elastic-ligament bridging and frictional pullout were found, similar to bridging processes observed in well-studied systems like Al_2O_3, Si_3N_4, and SiC [e.g., 16]. However, other striking bridging phenomena were observed, as shown in the FESEM image in Fig. 3. Here, heavily deformed lamellae were seen to bridge the crack, and significant amounts of delamination and bending were observed. The ligaments shown in Fig. 3 are further examples of the extent by which individual grains of Ti_3SiC_2 can deform [7]. This flexibility, typically absent in other layered compounds such as mica and graphite, can be traced to the metallic nature of the bonding and the absence of strong in-plane Si-Si bonds [13]. Such processes are highly unusual in ceramic systems and may, at least partially, account for the high steady-state fracture toughnesses by promoting very sizable bridging zone lengths (well over 5 mm in the coarse-grained microstructure).

Fatigue-Crack Propagation Behavior

In Fig. 4a, fatigue-crack growth rates are plotted as a function of the applied ΔK, for both the fine- and coarse-grained Ti_3SiC_2; results are compared with a range of metals and ceramics (all at $R = 0.1$, $\nu =$ 25 Hz, in room air). Although the very high dependence of *da*/*dN* on ΔK is typical for brittle solids,

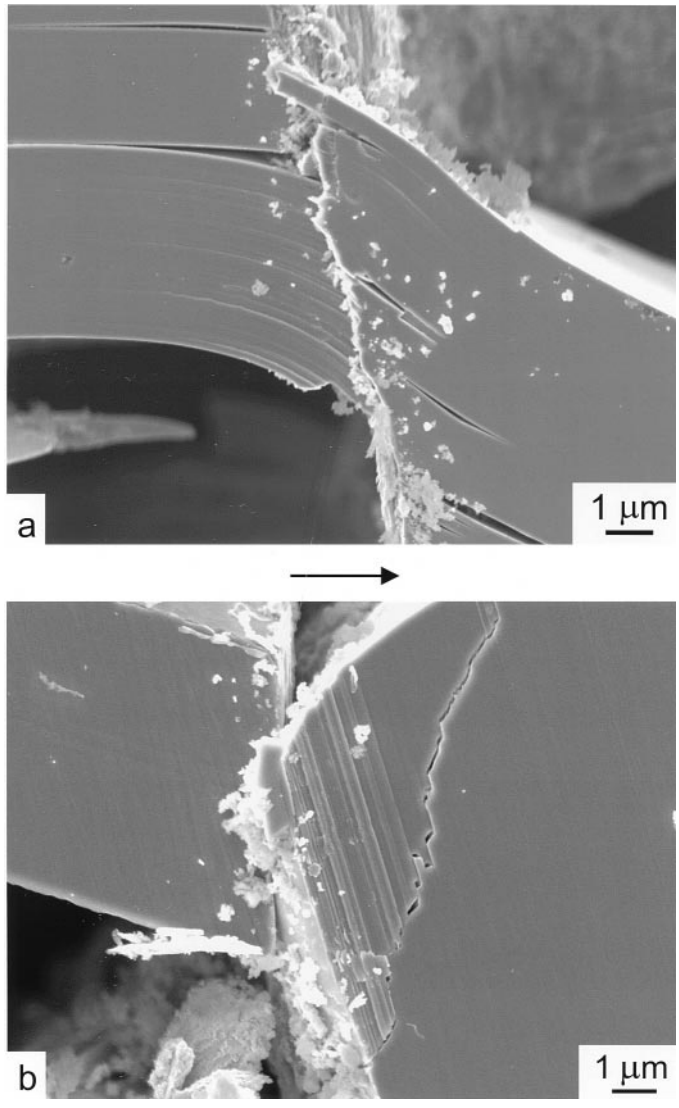

Figure 5. Field-emission scanning electron microscope images in (a) and (b) of fatigue damage behind the crack tip in a coarse-grained Ti_3SiC_2 specimen. Notice the appearance of wear debris along contacting surfaces. In (a), significant bending is observed, as well as delamination along basal planes. In (b), sliding along the contacting surface has generated shear-faulting along the basal planes of the grain on the right. The arrow indicates the direction of crack propagation.

growth rates in the coarse-grained Ti_3SiC_2 are lower and the ΔK_{TH} fatigue threshold is significantly higher ($\Delta K_{TH} \sim 9$ MPa$\sqrt{}$m) than other structural ceramics. Indeed, this ceramic exhibits some of the highest fatigue thresholds and cyclic-crack growth resistance ever observed in a monolithic, non-transforming ceramic. Typical of ceramic materials [20], the fatigue-crack growth rates scale directly with fracture toughness, as seen by comparing Figs. 1 and 4b. The fatigue threshold is somewhat lower ($\Delta K_{TH} \sim 6$ MPa$\sqrt{}$m) in the fine-grained microstructure, although the slopes of the growth-rate curves are quite similar.

FESEM images of fatigue damage behind the crack tip in a coarse-grained specimen revealed profuse amounts of wear debris along contacting surfaces (Fig. 5). Significant bending is apparent as well as delamination along basal planes (Fig. 5a). Furthermore, in Fig. 5b, sliding along the contacting surface of a bridge has generated shear-faulting along the basal planes of the grain on the right. Such shear-faulting may reduce the severity of frictional damage in these microstructures and help to account for the very high fatigue thresholds.

Summary and Conclusions

An experimental study of fracture and cyclic fatigue-crack growth behavior was made in a reactively hot-pressed monolithic Ti_3SiC_2 ceramic with both fine (3–10 μm) and coarse-grained (50–200 μm) microstructures. Whereas the fine-grained microstructure exhibited a steady-state (plateau) R-curve fracture toughness of $K_c \sim 9.5$ MPa$\sqrt{}$m, the coarse-grained Ti_3SiC_2 exhibited a $K_c \sim 16$ MPa$\sqrt{}$m. The latter value is thought to be one of the highest fracture toughnesses ever observed in a monolithic, non-transforming ceramic, consistent with the profusion of crack-bridging processes active in the crack wake. Moreover, fatigue-crack growth thresholds, ΔK_{TH}, were comparatively high for ceramic materials, as indicated by the coarse-grained microstructure which had a threshold ΔK_{TH} of $\sim$9 MPa$\sqrt{}$m. Such fatigue crack growth was associated with substantial evidence for wear degradation at active bridging sites behind the crack tip.

Acknowledgments

Work supported by the Office of Science, Office of Basic Energy Sciences, Materials Sciences Division, U.S. Department of Energy under Contract No. DE-AC03-76SF00098 (for the LBNL group), and by the Division of Materials Research, National Science Foundation, under Contract No. DMR 9705237 (for T.E-R. and M.W.B.).

References

1. M. W. Barsoum and T. El-Raghy, J. Am. Ceram. Soc. 79, 1953 (1996).
2. W. Jeitschko and H. Nowotny, Monatsch Chem. 98, 329 (1967).
3. B. R. Lawn and V. R. Howes, J. Mater. Sci. 16, 2745 (1981).
4. J. Lis, Y. Miyamoto, R. Pampuch, and K. Tanihata, Mater. Lett. 22, 163 (1995).
5. T. El-Raghy, A. Zavaliangos, M. W. Barsoum, and S. R. Kalidindi, J. Am. Ceram. Soc. 80, 513 (1997).
6. I. M. Low, S. K. Lee, B. R. Lawn, and M. W. Barsoum, J. Am. Ceram. Soc. 81, 225 (1998).
7. M. W. Barsoum and T. El-Raghy, Metall. Mater. Trans. A. 30A, 363 (1999).
8. L. Farber, M. W. Barsoum, A. Zavaliangos, and T. El-Raghy, J. Am. Ceram. Soc. 81, 1677 (1998).
9. M. W. Barsoum, L. Farber, and T. El-Raghy, Metall. Mater. Trans. A. 30A, 1727 (1999).
10. T. El-Raghy, M. W. Barsoum, A. Zavaliangos, and S. Kalidindi, J. Am. Ceram. Soc. 82, 2855 (1999).
11. A. T. Procopio, M. W. Barsoum, and T. El-Raghy, Metall. Mater. Trans. A. in press.
12. N. Tzenov and M. W. Barsoum, J. Am. Ceram. Soc. in press.
13. M. W. Barsoum, T. El-Raghy, C. J. Rawn, W. D. Porter, A. Payzant, and C. Hubbard, J. Phys. Chem. Solids. 60, 429 (1999).
14. P. L. Swanson, C. J. Fairbanks, B. R. Lawn, Y.-W. Mai, and B. J. Hockey, J. Am. Ceram. Soc. 70, 279 (1987).
15. C. W. Li, D. J. Lee, and S. C. Lui, J. Am. Ceram. Soc. 75, 1777 (1992).
16. C. J. Gilbert and R. O. Ritchie, Acta Mater. 46, 609 (1998).
17. R. H. Dauskardt, Acta Metall. Mater. 41, 2765 (1993).
18. S. Lathabai, J. Rödel, and B. R. Lawn, J. Am. Ceram. Soc. 74, 1340 (1991).
19. N. P. Padture and B. R. Lawn, Acta Metall. Mater. 43, 1609 (1995).
20. C. J. Gilbert and R. O. Ritchie, Fatigue Fract. Eng. Mat. Struct. 20, 1453 (1997).